Chapter 4

Precipitation Process in Fe-Ni-Al-based Alloys

Hector J. Dorantes-Rosales, Victor M. Lopez-Hirata,
Jorge L. Gonzalez-Velazquez,
Nicolas Cayetano-Castro and
Maribel L. Saucedo-Muñoz

Additional information is available at the end of the chapter

http://dx.doi.org/10.5772/61070

Abstract

This chapter covers first the precipitation and coarsening processes in Fe-Ni-Al alloys aged artificially at high temperatures, as well as their effect on the mechanical properties. These results show the precipitation evolution, morphology of precipitates, coarsening kinetics and mechanical properties such as hardness. Additionally, the effect of alloying elements such as copper and chromium is also studied on the precipitation and coarsening processes. The main results of this section are concerning on the coarsening kinetics and its effect on hardness. Besides, the diffusion couple method is employed to study the precipitation and coarsening process in different Fe-Ni-Al alloy compositions, as well as its effect on the hardness. All the above aspects of precipitation and coarsening are also supported with Thermo-Calc calculations.

Keywords: Fe-Ni-Al alloys, Beta prime phase, precipitation, aging, coarsening, hardness

1. Introduction

The Fe-Ni-Al system is very important for the design and development of several Fe-based alloys. For instance, the precipitation process of the β′ phase is relevant for the alloy strengthening at high temperatures in different engineering alloys such as PH stainless steels and Fe-Cr-Ni-Al-based alloys, etc. [1]. They are applied to fabricate different industrial components

which usually require a combination of good mechanical strength and oxidation resistance at elevated temperatures. The β′phase consists of an ordered phase of a NiAl type with a B2 (CsCl) crystalline structure. These alloys show excellent mechanical properties and corrosion resistance at high temperatures around 1000°C with a melting point of about 1638°C. They also have a density of about 5.7 g/cm^3 which is lower than that presented by the Ni-based superalloys, about 8 g/cm^3 [2].

In a similar way to Ni-superalloys, the Fe-based superalloys support its mechanical strengthening on the formation of coherent precipitates in a soft matrix. Likewise, the mechanical properties of precipitation hardened alloys are closely related to the morphology, spatial distribution, volumetric fraction and average radius of the precipitated particles in the phase matrix. These microstructural characteristics can be controlled by means of heat treatments; however, they are also modified during the operation of industrial components at high temperatures for prolonged times [3–6].

The coarsening process is a metallurgical phenomenon which takes place at high temperatures and consists of the dissolution of small precipitates and subsequent mass transfer to the larger precipitates during the heating of alloys. This phenomenon usually has a strong effect on the mechanical properties of alloys. The Lifshitz-Slyozov-Wagner (LSW) theory for diffusion-controlled coarsening predicts a coarsening growth kinetics with a time dependent of $t^{1/3}$ considering the spherical precipitates without elastic interaction with the phase matrix and precipitate volume fraction close to zero [7,8]. There are several modified LSW theories for diffusion-controlled coarsening which incorporated higher volume fractions and the precipitate morphology different from spheres, as well as multicomponent alloys. Nevertheless, the temporal power law of $t^{1/3}$ is sustained in all the above cases, but the time-independent precipitate size distribution of LSW theory becomes broader and more symmetric with the increase in volume fraction [9–13]. The coarsening resistance of precipitates is a very important factor to retain a good strength at high temperatures in these alloys. An alternative to have a better coarsening resistance, it can be obtained either by a low value of lattice misfit which maintains a coherent interface with low interfacial energy between the precipitate and the matrix, low solute solubility or slow atomic diffusion in the matrix phase [13]. The addition of alloying elements is a good alternative to control the coarsening kinetics because of its effect on the interfacial energy, solubility of precipitates or atomic diffusion. For instance, the addition of Cu is expected to have, at least, effect on the solubility since Cu has low solubility in bcc Fe and it has a good solubility in Ni and more than 4 at.% in Al [14]. A small addition of Cu to the Fe-Ni-Al alloys is expected to modify the coarsening kinetics of β′ precipitates. Another possibility is the chromium addition which has a higher solubility in the ferrite matrix and thus it could also influence on the coarsening kinetics [15].

The precipitation and coarsening process are usually analyzed by artificial aging of a given composition alloy. Nevertheless, an alternative way for studying the precipitation reactions in ternary alloys is using diffusion couples [16–17] which permit to analyze the precipitation process for different alloy compositions in the same specimen. This method has been used to determine solubility limits and precipitation evolution which is based on the microstructure observation of different composition aged alloys produced by a continuous composition

gradient in the specimen. There are different methods to create the macroscopic composition gradient in the specimen such as diffusion couples, imperfect arc melting of sandwiched metals, imperfect homogenization of coarse precipitates, etc. This method has also been applied to study the precipitation and coarsening processes in Fe-Ni-Al alloys [18].

Thus the studies of precipitation process in Fe-Ni-Al alloys can be summarized as follows: The precipitation of the NiAl type β′ phase in an Fe-rich phase matrix has been analyzed in different works [5,6]. The effect of alloying elements on the precipitation process and its mechanical properties has been also studied by different authors [3,4,14,15]. The application of diffusion couples to analyze the precipitation process in Fe-Ni-Al alloys has been reported in the literature [15].

Therefore, the present chapter covers first the precipitation and coarsening processes in Fe-Ni-Al alloys aged artificially at high temperatures, as well as their effect on the mechanical properties. These results show the precipitation evolution, morphology of precipitates, coarsening kinetics and mechanical properties such as hardness. Additionally, the effect of alloying elements such as copper and chromium is also studied on the precipitation and coarsening processes. The main results of this section are concerning on the coarsening kinetics and its effect on hardness. Besides, the diffusion couple method is employed to study the precipitation and coarsening process in different Fe-Ni-Al alloy compositions, as well as its effect on the hardness. All the above aspects of precipitation and coarsening are also supported with Thermo-Calc calculations.

2. Phase diagrams of Fe-Ni-Al system

Figures 1 (a–d) show the calculated isothermal ternary phase diagrams of the Fe-Ni-Al system corresponding to 750, 850, 950 and 1100°C, respectively [19]. In general, it can be seen that the liquid and ferrite phase regions decrease with the decrease in temperature. The β′ phase region increases as temperature increases. The austenite phase region also shows an increase as temperature increases. The γ′ phase also extends its presence as temperature decreases. These diagrams show good agreement with the experimental ones reported in the literature [5,20].

If chromium is added to the above ternary system, some changes may occur since this has an extended solubility in both the austenite and the ferrite phases. The calculated pseudo-ternary Fe-Ni-Al phase diagrams with the addition of 1 wt.% Cr are shown in Figures 2 (a–d) for 750, 850, 950 and 1100°C, respectively. It can be noticed, in general, that the β′ phase region increases as temperature decreases from 1100°C to 950°C, and then it decreases from 850°C to 750 °C. The ferrite phase region also increases with temperature, but it is slightly wider than that of the ternary system. The β′ and liquid region are not present for the four temperatures. The austenite phase region also increases with temperature and the γ′ phase region increases as temperature decreases. There are no experimental data reported in the literature for comparison.

3. Precipitation process

According to the ternary phase diagram, shown in Figure 1, it is possible to carry out a hardening precipitation treatment in the Fe-rich region. Even more, the precipitation reaction can take place in two ways [20]:

$$\beta' \rightarrow \beta' + \alpha \tag{1}$$

$$\alpha \rightarrow \alpha + \beta' \tag{2}$$

That is, the supersaturated solid solution of either the β′ or α phase can produce a mixture of the ferrite α phase and the ordered intermetallic β′ phase which can promote an increase in the mechanical strength and thus a better performance in creep conditions. Additionally, it is expected to have a coherent interface between these two phases since the lattice parameter of these is very similar [3]. Additionally, this fact gives better creep resistance in this type of alloys.

For instance, the X-ray pattern for the Fe-10wt.%Ni-15wt.%Al alloy solution treated at 1100 °C and then aged at 850 °C for 5 h is shown in Figure 3. The XRD pattern for the solution treated specimen only indicates the peaks from the bcc ferritic α phase. On the other hand, the XRD pattern corresponding to the aged specimens shows the main reflections corresponding to the ordered NiAl-type β′ phase. The principal morphology characteristics of precipitation in Fe-rich Fe-Ni-Al alloys is the presence of cuboids of the β′ phase dispersed in the ferrite matrix showing a preferential alignment on the <100> directions of the ferritic α phase due to the lowest elastic-strain energy [13]. This alignment can be clearly observed in the DF-TEM micrograph of the Fe-10wt.%Ni-15wt.%Al alloy aged at 850 °C for different times and its corresponding electron diffraction pattern with a zone axis [100] shown in Figure 4.

4. Microstructure evolution during coarsening

An important characteristic for an alloy with good creep resistance is that the interparticle distance between the β′ precipitates should be as short as possible. Thus, it is important to know the microstructure evolution of precipitates during the coarsening stage, as well as its kinetics and the effect on the mechanical properties of creep resistance alloys.

As an example, the precipitation evolution during the coarsening process for the Fe-10wt.%Ni-15wt.%Al, Fe-10wt.%Ni-15wt.%Al-1wt.%Cr and Fe-10wt.%Ni-15wt.%Al-1wt.%Cu alloys is shown in Figures 5, 6 and 7 (a–f), respectively. The morphology of the β′precipitates is rounded cuboids in the three aged alloys from the early stages of aging at all temperatures, Figures 5–7 (a–c).The straight sides of precipitates suggest the presence of a coherent interface between the precipitates and the matrix.

http://dx.doi.org/10.5772/61070

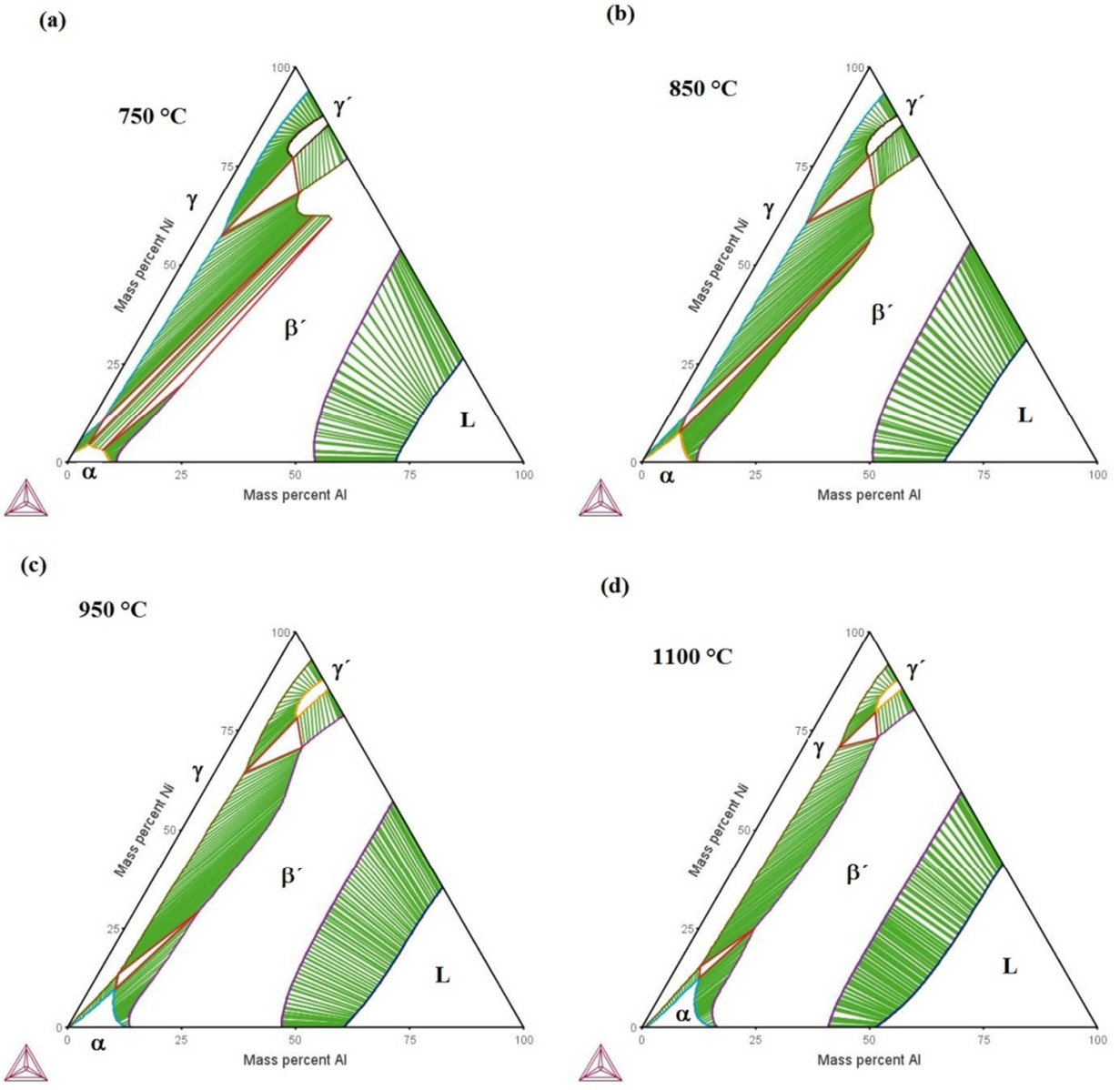

Figure 1. Calculated isothermal phase diagrams of the ternary Fe-Ni-Al system at (a) 750°C, (b) 850°C, (c) 950°C and (d) 1100°C.

The precipitates become aligned with the ferritic matrix over the course of time, Figures 5 (c–d).This alignment has been reported [13] to occur in the <100> crystallographic direction of the ferrite matrix since it corresponds to the softest one in the bcc crystalline structure. This suggests that the alloy specimens have the <100> orientation in the aged specimens. A further aging promotes the increase in size of precipitates in both of the aged alloys. The increase in precipitate size is higher as the aging temperature increases. Aging for longer times has a tendency to form square or rectangular arrays of cuboid precipitates in both alloys; however, this fact seems to be higher in the ternary alloy aged at 750°C and 850°C than that in the other one, Figure 5 (e,f).

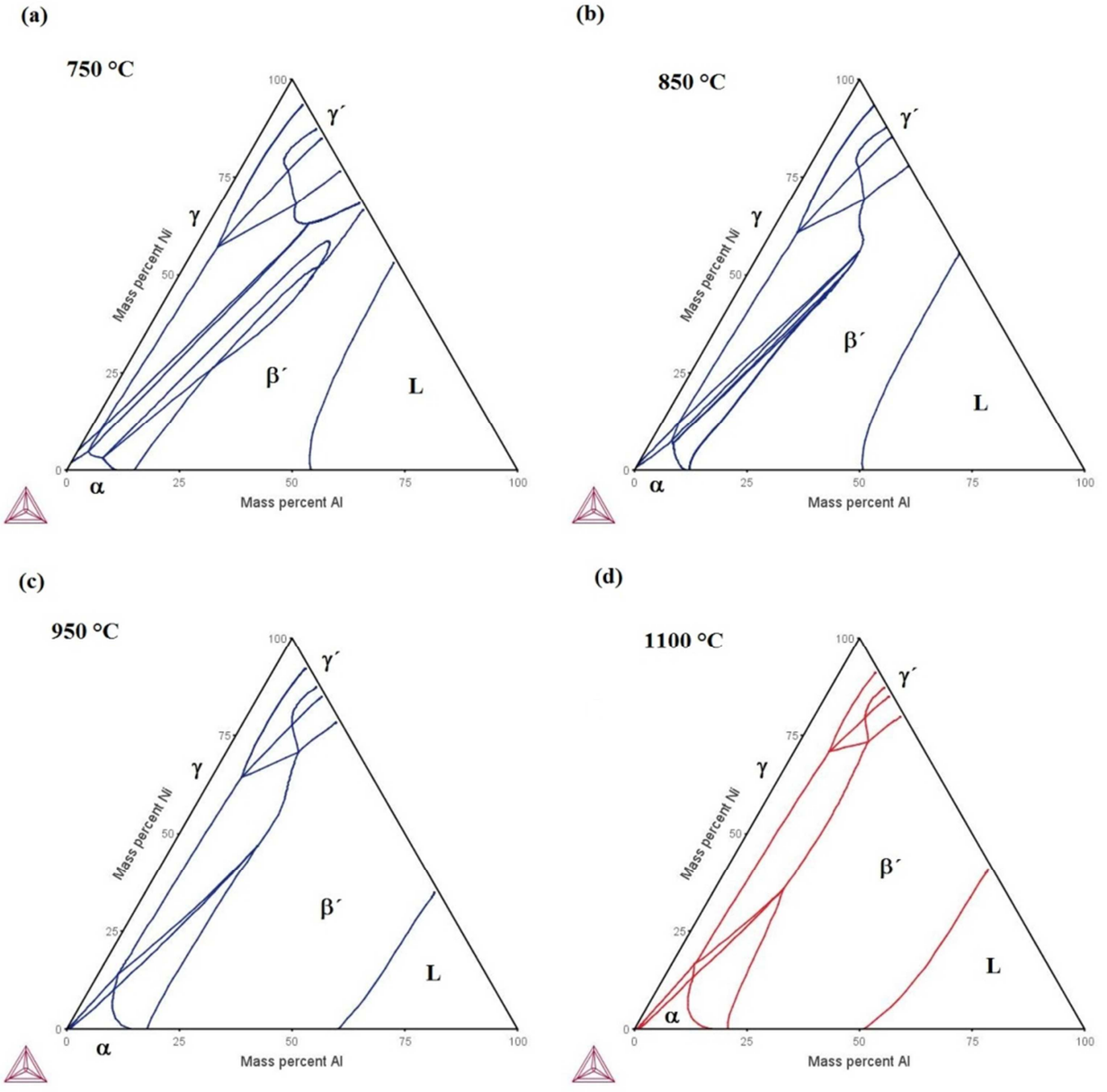

Figure 2. Isothermal phase diagrams of the pseudo-ternary Fe-Ni-Al-1wt.%Cr system at (a) 750°C, (b) 850°C, (c) 950°C and (d) 1100°C.

At aging at 950°C, elongated arrays of precipitates are aligned with respect to the ferritic matrix in the aged alloys, Figures 5, 6 and 7 (f–i). Some coalescence of precipitates is observed in these arrays and the straight sides of some precipitates become curved. This suggests the loss of coherency between the precipitates and the matrix. This characteristic is more notorious in the case of the aged ternary alloy. This behavior seems to be related to a higher elastic-strain effect in this alloy [13]. No splitting of precipitates was observed to occur in the aged alloys. The volume fraction is, in general, higher for the ternary alloy; however, the volume fractions are very close in alloys aged at 750°C. It is interesting to notice that the end of plates is like a rounded-tip for the aged Fe-10wt.%Ni-15wt.%Al-1wt.%Cu alloy, while it is more or less flat

http://dx.doi.org/10.5772/61070

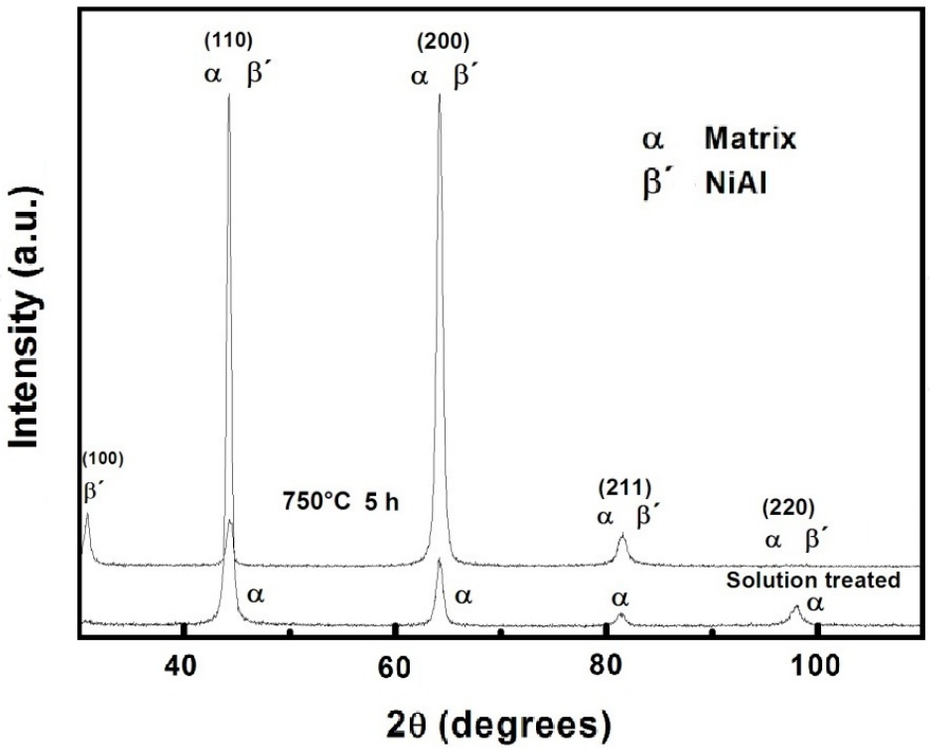

Figure 3. XRD pattern of the Fe-10wt.%Ni-15wt.%Al alloy solution treated at 1100°C and then aged at 850°C for 5 h.

for the other aged alloys. This fact suggests that the coherency between matrix and precipitates is lost in the former alloy and thus the plate grows more easily in that direction. This causes a larger length of plates in this case. The alignment of precipitates on elastically softest directions occurred faster in the Cu-containing alloy. This can be attributed to a higher coherency-strain energy which may be caused by a larger lattice misfit because of the Cu addition.

5. Coarsening kinetics

The coarsening kinetics of precipitates is usually an important parameter to analyze the creep resistance in the heat-resistant alloys, as well as to know the effect of alloying elements on the coarsening process of precipitates, which enables us to design better creep resistance alloys. The conventional way for analyzing the coarsening kinetics is to plot the equivalent radius, determined from the area of a precipitate, against

the aging time. The variation of radius r with time t obeys usually a power law, $r = kt^n$, and the time exponent usually indicates the coarsening mechanism. The Lyfshitz-Slyozov-Wagner (LSW) theory for diffusion-controlled coarsening rules the coarsening behavior of precipitates in different alloys [7–13].

Furthermore, several modifications of this theory have been reported [13] to consider the shape, volume fraction and coherency effects on the growth kinetics.

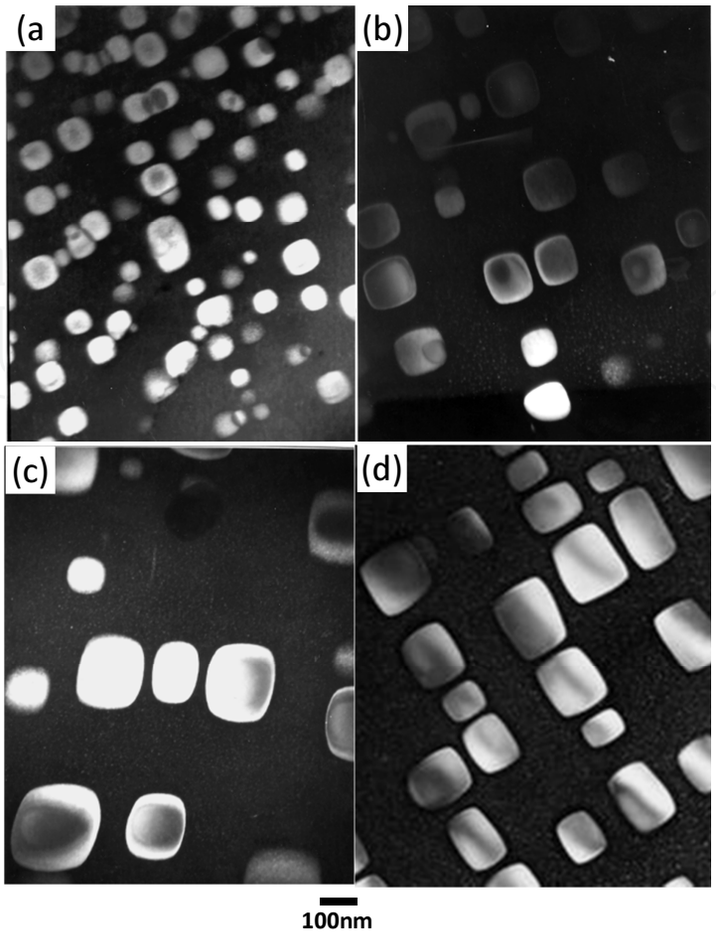

Figure 4. DF-TEM micrograph and electron diffraction pattern for the Fe-10wt.%Ni-15wt.%Al alloy aged at 850°C for (a) 1 h, (b) 5 h, (c) 25 h and (d)75 h.

To show the coarsening kinetics in Fe-Ni-Al alloys, the average equivalent circus radius, *r*, of β′ precipitates, expressed as r^3- r_o^3, is plotted as a function of aging time in Figure 8 (a–c)for the aged Fe-10wt.%Ni-15wt.%Al, Fe-10wt.%Ni-15wt.%Al-1wt.%Cr and Fe-10wt.%Ni-15wt. %Al-1wt.%Cu alloys, respectively. These figures show straight line curves for the different cases which suggest that the LSW theory for diffusion-controlled coarsening is followed in this study. The LSW theory and modified LSW theories [7,13] express mathematically the variation of particle radius with time as follows:

$$r^3 - r_o^3 = kt \tag{3}$$

where r_o and r are the average radius of precipitates at the onset of coarsening and time t, respectively, and k is a rate constant which can be determined from the slope of straight lines in Figure 8. The r_o value was determined from the linear regression analysis for each case. Figure 8 also shows the values of rate constant k for each case and they indicate that the coarsening process takes place more rapidly for the Fe-10wt.%Ni-15wt.%Al alloy aged at the three temperatures than that of the other two alloys. In general, the slowest growth kinetics

http://dx.doi.org/10.5772/61070

can be observed for the aged Fe-10wt.%Ni-15wt.%Al-1wt.%Cr alloy. This behavior suggests the effect of chromium and copper on the Ostwald ripening process in this alloy.

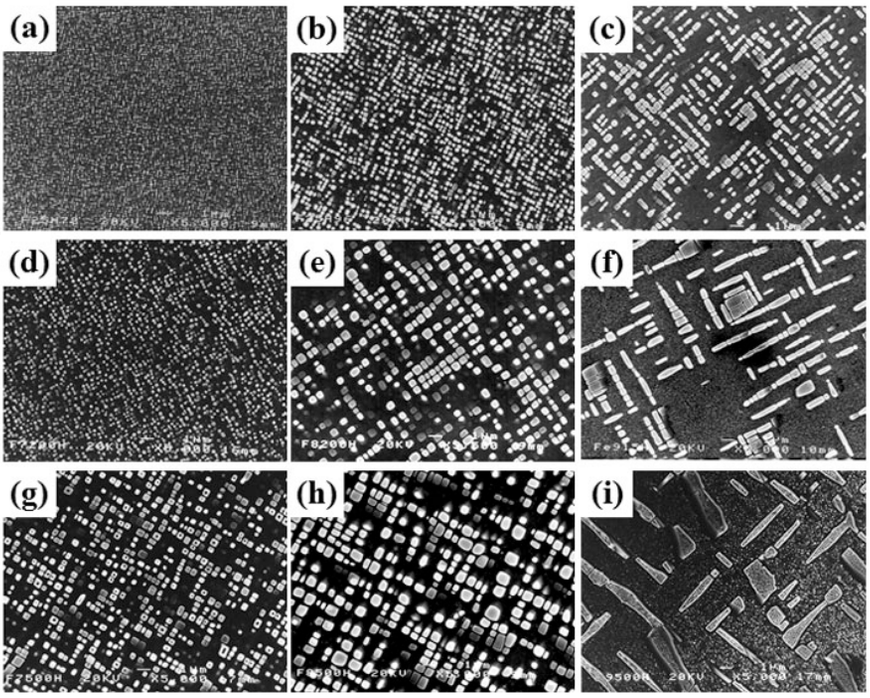

Figure 5. SEM micrographs of the precipitation evolution for the Fe-10wt.%Ni-15wt.%Al alloy aged at (a,d.g) 750°C, (b,e,h) 850°C and (c,f,i) 950°C for 25, 200 and 500 h, respectively.

A further analysis of the rate constant *k* can be conducted by obtaining the Arrhenius plot of this, as shown in Figure 9. The slope from the straight lines permits to determine the activation energy for the coarsening of β′precipitates in each alloy. It can be noticed that the lowest value corresponds to the ternary alloy and the highest energy is for the aged Fe-10wt.%Ni-15wt. %Al-1wt.%Cu alloy. This is in agreement with the fastest and lowest coarsening kinetics, respectively, observed in these two alloys. The activation energy is in the range of 200–240 kJ/mol, which is close to the value of 188 and 234 kJ/mol reported for the bcc Fe-rich Fe-Al alloys [21]. In order to understand the effect of alloying element on the coarsening process in these alloys, Figure 10 (a) illustrates the HAADF-STEM image of the Fe-10wt.%Ni-15wt.%Al-1wt. %Cr alloy aged at 950°C for 50 h. Some β′ precipitates and the ferrite matrix can be observed in the micrograph. The STEM intensity profile corresponding to Fe, Ni, Al and Cr elements, following the line A to B indicated in Figure 10 (a), are shown in Figure 10 (b). The presence of chromium is slightly higher in the ferrite matrix than that observed in the β′ precipitates. The iron content of precipitates is higher than that of nickel and aluminum. In order to show more clearly the effect of alloying elements, a Thermo-Calc equilibrium analysis [19] was carried out for the two alloy compositions at temperatures between 750°C and 950°C. Thermo-Calc analysis indicates that the ferrite matrix is richer in chromium, about 1.1 at.% for all temperatures, in comparison with that in the β′ precipitates. This detail is in good agreement

with the chemical behavior reported in the literature for Fe-Ni-Al-Cr alloys [3]. The mole fraction of alloying elements is shown in Figure 11 for the equilibrium β′ phase for the Fe-10wt.%Ni-15wt.%Al and Fe-10wt.%Ni-15wt.%Al-1wt.%Cr alloys at temperatures between 750°C and 950°C. These precipitates are expected [2] to be an (Fe,Ni)Al intermetallic compound. Thermo-Calc analysis shows that the iron content in the β′ precipitates increases with the aging temperature, from about 10 to 50 at.%, while the nickel and aluminum contents decrease with temperature, from about 45 to 20 at.% in both alloys. However, the content of iron in the β′ precipitates is slightly lower in the Fe-10wt.%Ni-15wt.%Al-1wt.%Cr alloy than that corresponding to the other alloy, while the nickel and aluminum contents of the former alloy are slightly higher than that of the latter alloy. In the case of the alloy with chromium, the chromium contents show a slight increase with temperature, from 0.04 to 0.22 at.%. This chemical behavior suggests that the β′ precipitates are an intermetallic compound closer to the NiAl compound in both alloys aged at 750°C since the Fe content is low. In contrast¸ the β′ precipitates are a compound of (Fe,Ni)Al type in both alloys aged at 850°C and 950°C showing a considerable amount of iron, which is in good agreement with Figure 5. This behavior may be favorable for having a higher coarsening resistance in these precipitates since the atomic diffusion process would be more complex which may cause its retardation [13]. As mentioned above, the coarsening resistance in the alloy with chromium is higher than that observed in the other alloy. This fact can be attributed mainly to the presence of chromium in both the ferrite matrix and the β′ precipitates which cause a slower diffusion process during the coarsening of precipitates.

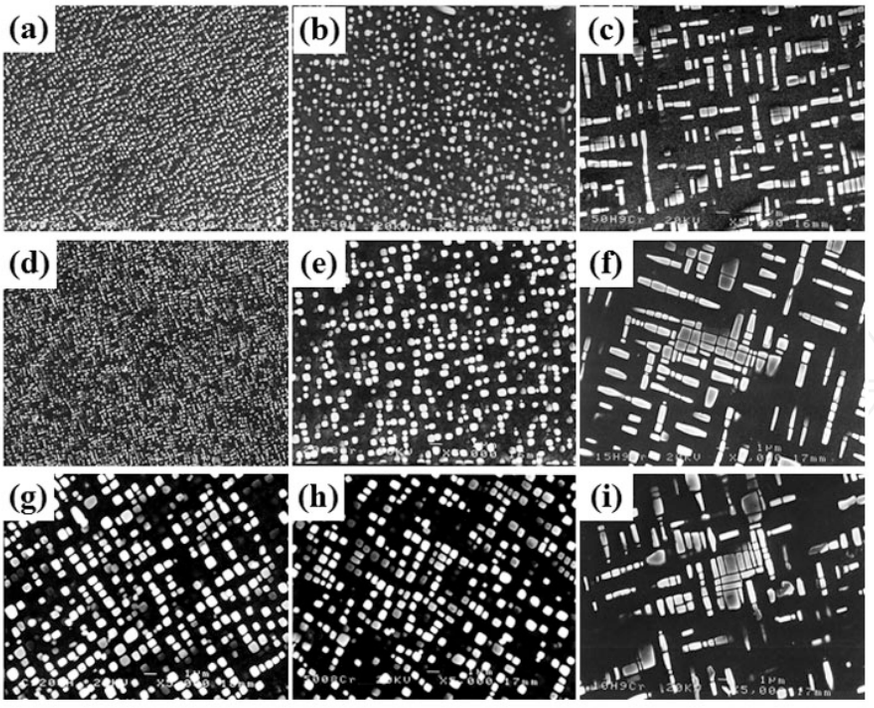

Figure 6. SEM micrographs of the precipitation evolution for the Fe-10wt.%Ni-15wt.%Al-1wt.%Cr alloy aged at (a,d.g) 750°C, (b,e,h) 850°C and (c,f,i) 950°C for 25, 200 and 500 h, respectively.

http://dx.doi.org/10.5772/61070

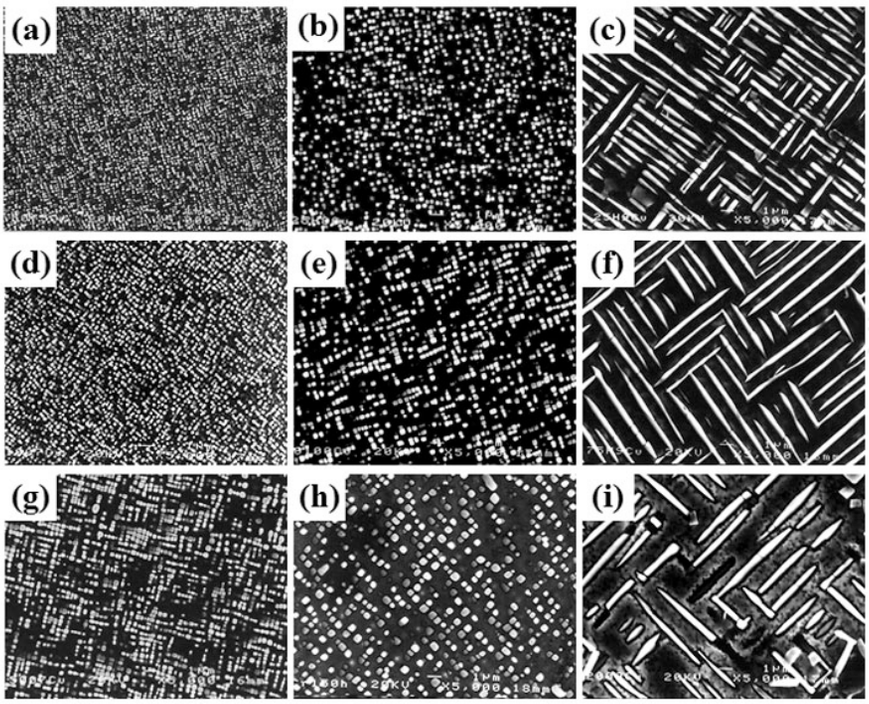

Figure 7. SEM micrographs of the precipitation evolution for the Fe-10wt.%Ni-15wt.%Al-1wt.%Cu alloy aged at aged at (a,d.g) 750, (b,e,h) 850 and (c,f,i) 950 °C for 25, 75 and 200 h, respectively.

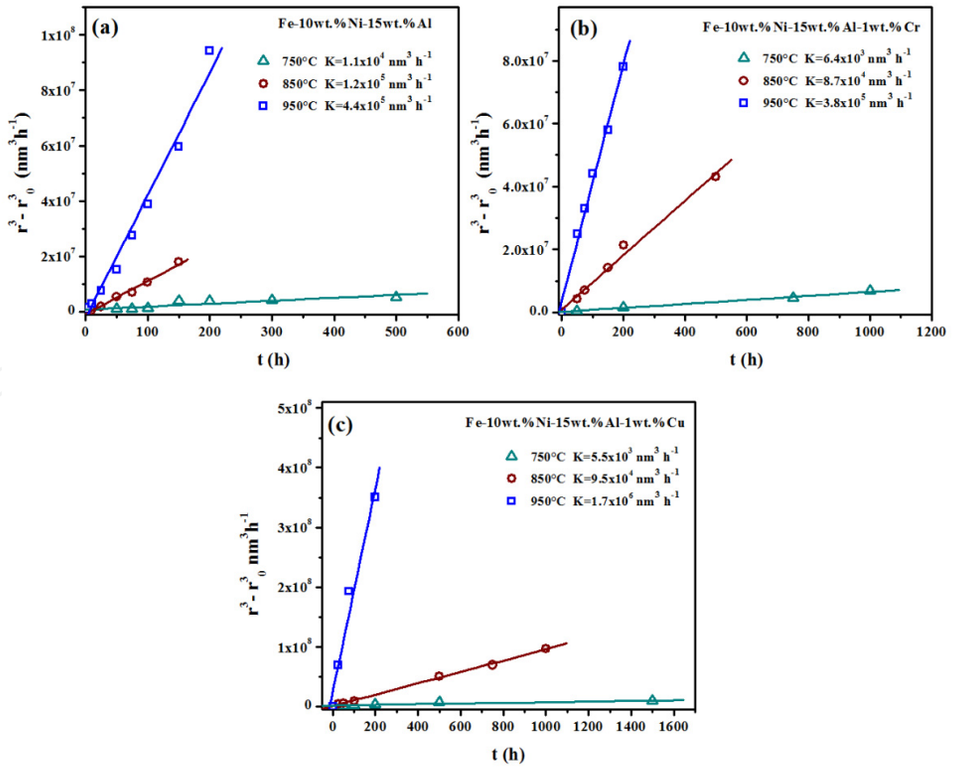

Figure 8. Plot of the cube equivalent radius as a function of aging time.

Figure 12 (a) shows a HAADF-STEM image of the Fe-10wt.%Ni-15wt.%Al-1wt.%Cu alloys aged at 750°C for 100 h. The corresponding HAADF-STEM EDS line scan profile is also shown in Figure 12 (b) for this specimen. The Fe-rich content of the ferritic matrix is evident. In contrast, the β′ precipitates are composed of Fe, Ni, Al and Cu. Furthermore, most of the Cu content is located within the β′ precipitates. This fact suggests a delay in the volume diffusion and thus, the coarsening resistance seems to be improved.

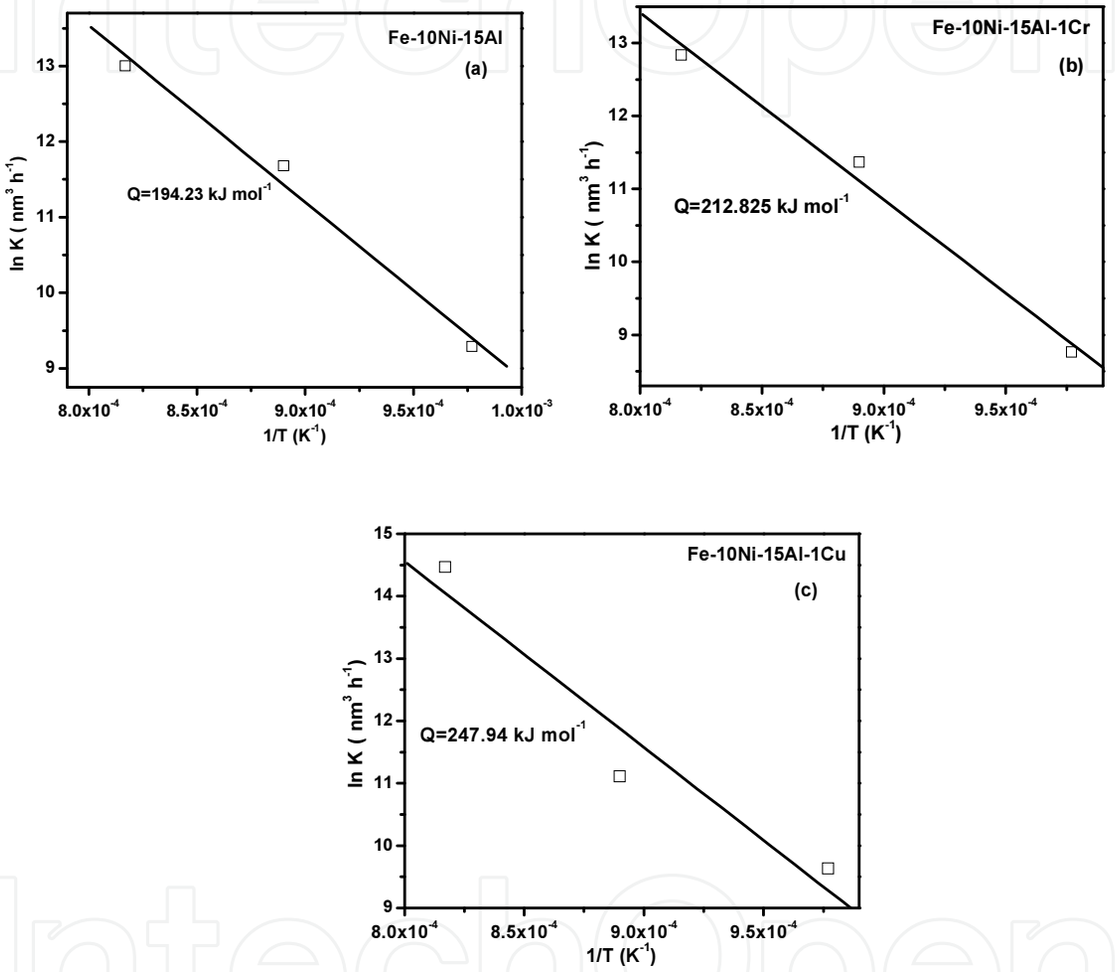

Figure 9. Arrhenius plot of the rate constant *k*.

The probability density $\rho^2 h(\rho)$ was determined with the following equation [14,15]:

$$\rho^2 f(\rho) = \frac{N_{(r,r+\Delta r)}}{\sum N_{(r,r+\Delta r)}} \frac{\bar{r}}{\Delta r} \frac{9}{4} \tag{4}$$

where r is the average radius of particles and $N_i(r+\Delta r)$ indicates the particle number in a given radius interval Δr. The normalized radius is defined as the ratio of $r / \bar{r}$. It can be noticed that

the particle size distribution is broader and lower than the size distribution predicted by the LSW theory in the alloys aged for prolonged times, while it is more similar to that predicted by the LSW theory for short aging times.

The precipitate size distribution, plot of the probability density versus the normalized radius ϱ, is shown in Figures 13 (a–f)for the Fe-10wt.%Ni-15wt.%Al, Fe-10wt.%Ni-15wt.%Al-1wt.%Cr and Fe-10wt.%Ni-15wt.%Al-1wt.%Cu alloys, respectively, aged at 750°C for 50 and at 950°C for 150 h. The size distribution of the LSW theory for diffusion-controlled coarsening is also shown in these figures. The size distribution of both alloys, aged at 750°C for 50 h, is more symmetrical and closer to that one of LSW theory. In contrast, the size distribution of both alloys, aged at 950°C for 150 h, is broader and more symmetrical, which is a coarsening characteristic observed in different binary and ternary alloys, either with large volume fraction of precipitates or with high coherency-elastic strain effect [12,13]. This behavior is in complete agreement with the size distribution predicted using the modified LSW theories [11].

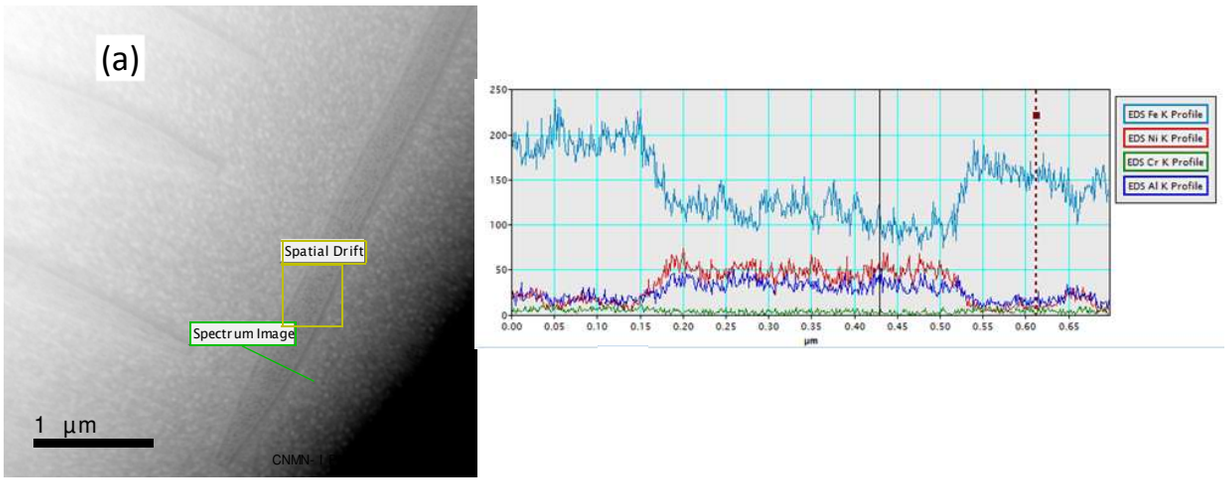

Figure 10. (a) HAADF-STEM image of (Fe,Ni)Al precipitates in a Fe matrix and (b) intensity profile of Fe, Ni, Al and Cr elements.

6. Hardness of aged alloys

The aging curves are shown in Figure 14 for the three alloys aged at 750, 850 and 950°C. The highest hardness corresponds to the aged Fe-10wt.%Ni-15wt.%Al-1wt.%Cu alloy, while the lowest one is observed to occur in the aged Fe-10wt.%Ni-15wt.%Al alloy. This hardness can be related to the presence of a small amount of copper in the β′ precipitates, Figure 11. In the case of Fe-10wt.%Ni-15wt.%Al-1wt.%Cr alloy, the increase in Fe content for the β′precipitates has been reported [3,4] to cause an increase in strength, while its decrease tends to improve its ductility. The highest resistance to the overaging in these alloys occurs during the aging at 750°C, which shows the slowest coarsening kinetics in both alloys. In contrast, the lowest coarsening resistance was observed to take place in the highest aging temperature because of the fastest Ostwald ripening process [13].

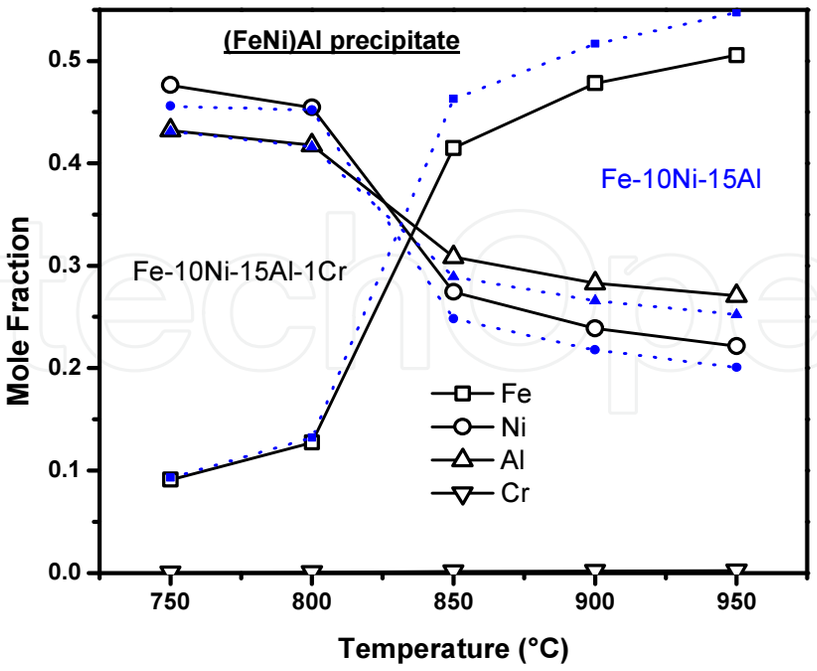

Figure 11. Calculated fraction mole of alloying elements in the β´precipitates against aging temperature for the Fe-10wt.%Ni-15wt.%Al and Fe-10wt.%Ni-15wt.%Al-1wt.%Cr alloys.

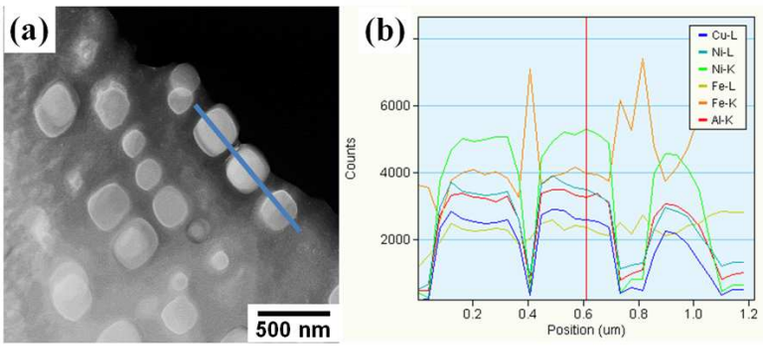

Figure 12. (a) HAADF-STEM image of (Fe,Ni)Al precipitates in a Fe matrix and (b) intensity profile of Fe, Ni, Al and Cu elements.

7. Application of diffusion couples

An alternative way for studying the precipitation reactions in ternary alloys is using diffusion couples which permit to analyze the precipitation process for different alloy compositions in the same specimen [16,17]. Furthermore, the diffusion couples have been used widely to study the precipitation process in binary alloys. This technique is called macroscopic composition gradient method. This procedure permits to determine solubility limits and precipitation evolution and it is based on the microstructure analysis of different composition alloys formed

http://dx.doi.org/10.5772/61070

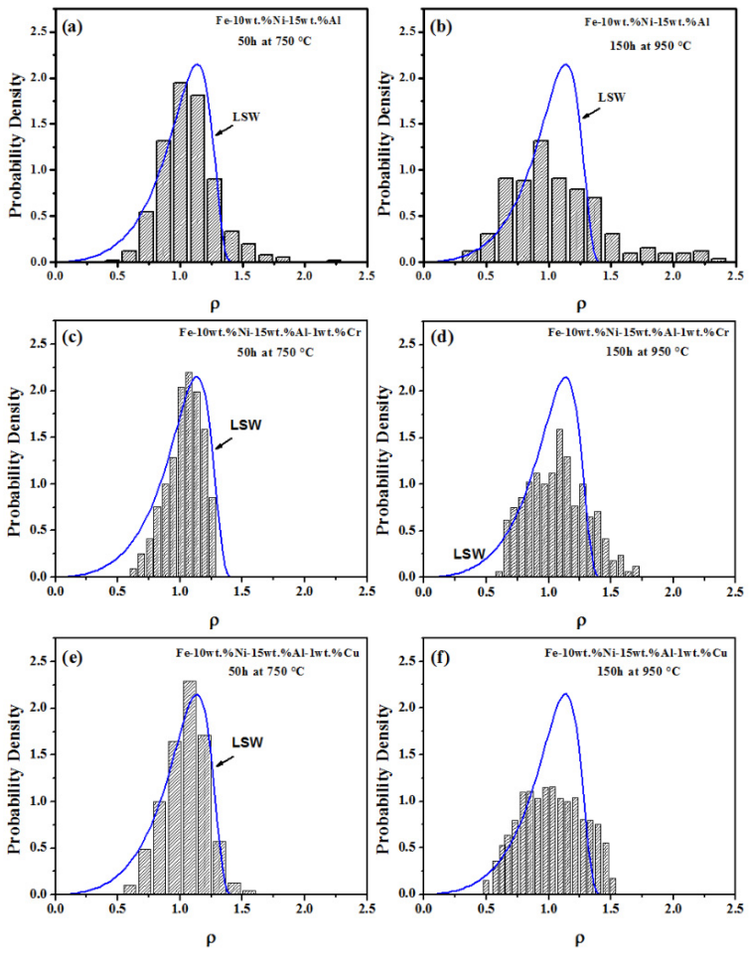

Figure 13. Precipitate size distributions for the (a–b) Fe-10wt.%Ni-15wt.%Al, (c-d) Fe-10wt.%Ni-15wt.%Al-1wt.%Cu and (e–f) Fe-10wt.%Ni-15wt.%Al-1wt.%Cr alloys aged at 750°C and 950°C for 50 and 150 h, respectively.

by a continuous composition gradient. The macroscopic composition gradient can be created in a specimen by different methods as stated above.

Figure 15 shows the Fe-25at.%Ni-25at.% Al alloy /Fe diffusion couple after diffusion heat treatment at 1100°C for 96 h. The black arrows indicate the interface of diffusion couple while dotted arrow indicates the path of linear chemical analysis with EDS. The concentration profiles of Fe, Ni and Al are shown in Figure 15.

The zero value in the x-axis is the position of the diffusion couple interface. The concentration profiles show that a composition gradient is present from the interface on both sides of the diffusion couple. That is, the Ni and Al compositions decrease toward Fe side, while the iron content decreases towards the alloy side. This profile behavior indicates that interdiffusion process occurs from high to low concentration regions.

The precipitation evolution is shown in Figure 16 for the diffusion couple solution treated and then aged at 900°C for different times. The SEM micrographs correspond to six different zones in the diffusion couple, designated as C_1–C_6. The Al and Ni contents increase from position

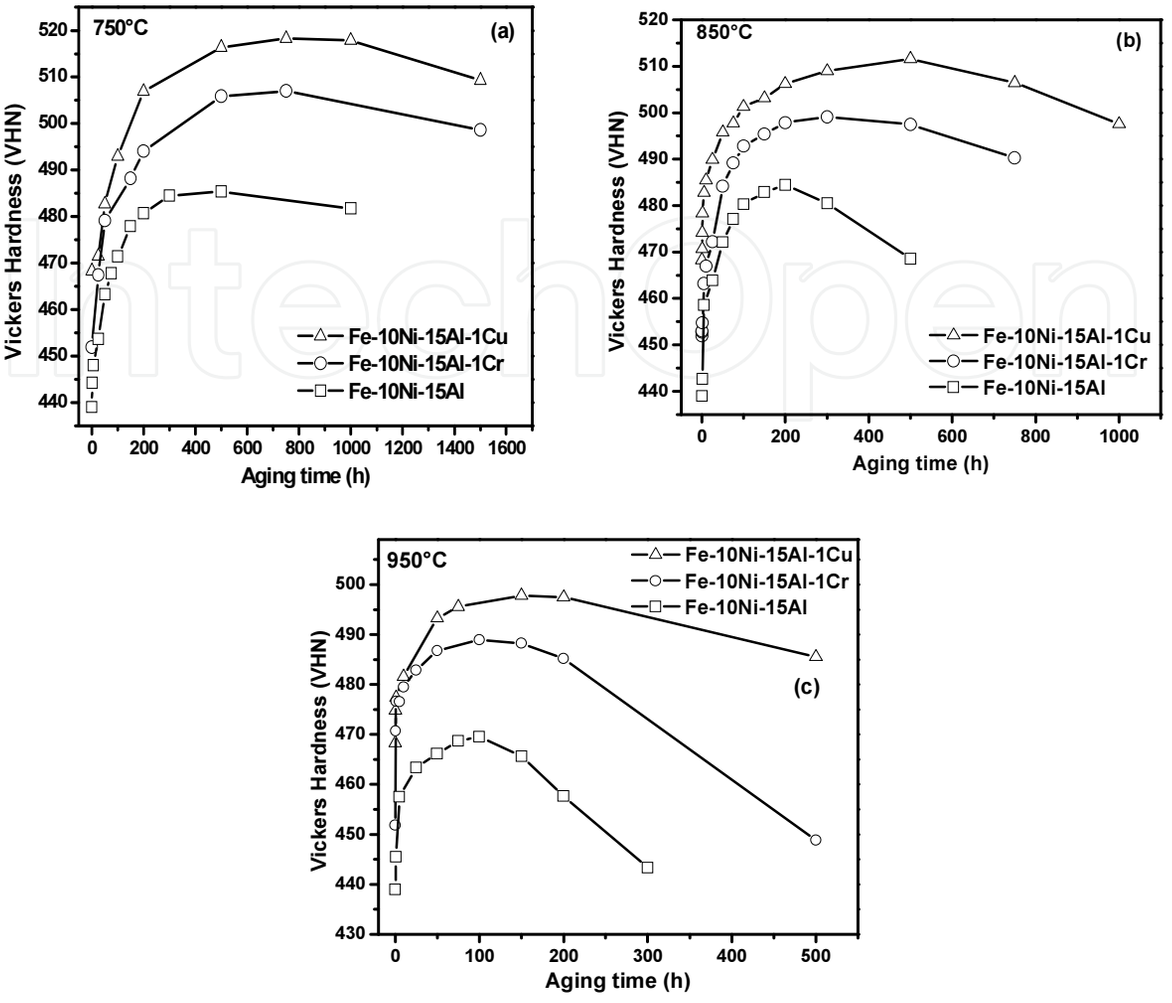

Figure 14. Aging curves for the Fe-10wt.%Ni-15wt.%Al, Fe-10wt.%Ni-15wt.%Al-1wt.%Cu and Fe-10wt.%Ni-15wt.%Al-1wt.%Cr alloys aged at 750, 850 and 950°C.

C_1 to positionC_6, as shown in Table 1. It is important to mention that the solution-treated diffusion couple indicated almost no precipitation. The precipitate morphology is rounded cuboids at the initial stages of aging. The cuboid precipitates seem to be aligned in a given crystallographic direction of the ferrite phase matrix. According to the literature [15], this direction correspond to the <100> direction of the ferrite matrix with the intention of decreasing the coherency-strain energy.

The X-ray diffraction patterns for the solution-treated and then aged alloy side in the diffusion couple are shown in Figure 17. A single-phase, the ferrite phase, is confirmed in the solution-treated specimen, while the presence of the XRD peaks corresponding to the β phase is clearly detected in the XRD pattern of the diffusion couple aged at 900°C for 50 h. No other phases were detected.

The volume fraction of precipitates increases with the increase in Ni and Al contents. As the aging progresses, the precipitate coarsening for all composition positions can be noted.

http://dx.doi.org/10.5772/61070

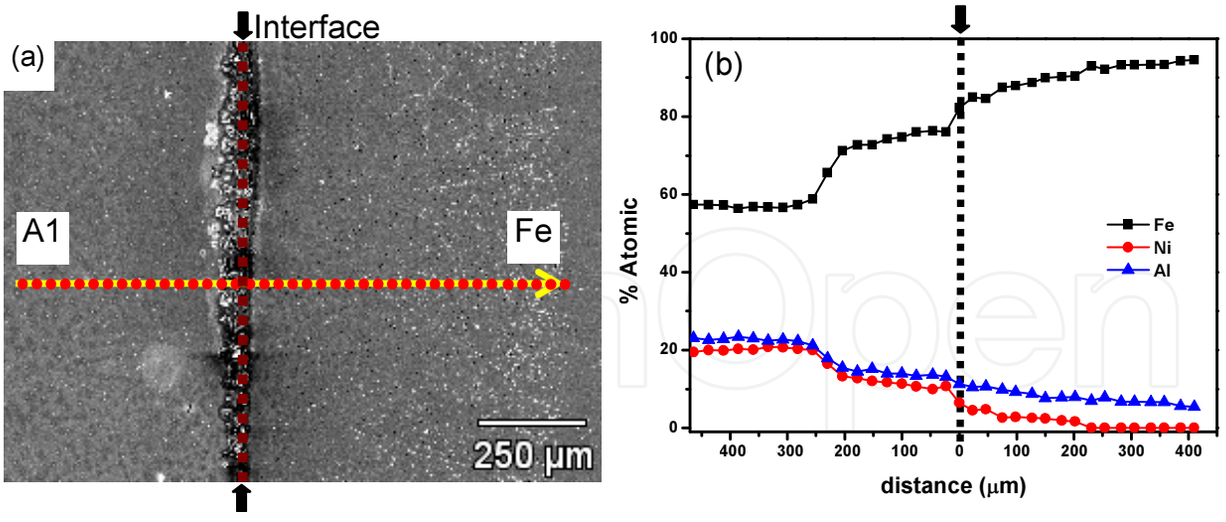

Figure 15. SEM micrograph of the (a) diffusion couple and (b) EDS chemical composition.

As a result of prolonged aging, the precipitate morphology becomes elongated and irregular. The coarsening process is observed to take place firstly in the zones which have higher content of solutes. This fact can be associated with the higher precipitate volume fraction which facilitates the coarsening process [13]. It is important to notice that the precipitate faces are curved in this stage of aging. This could indicate the coherency between the precipitates and the matrix. This fact can be adopted as the reason for the faster coarsening kinetics of the elongated precipitates.

For the first four compositions C_1–C_4, the precipitate radii r were measured, taking into account only precipitates with rounded cuboid shape, at any aging time t. The plot of ln r vs. ln t is shown in Figure 18. The coarsening growth kinetics is expected to follow this equation [7, 13]:

$$r = k_r t^n \tag{5}$$

where r and t are the mean radius of precipitates and time t, respectively, k_r is a rate constant and n the time exponent. The slope value n can be obtained from Figure 18 and these were 0.29, 0.29, 0.30 and 0.31 for the compositions C_1 to C_4, respectively. These values are close to 1/3 which is predicted by the diffusion-controlled coarsening LSW theory [8] and the modified LSW theory for ternary alloys [10]:

$$r^3 - r_o^3 = k_r t \tag{6}$$

where r_o and r are the mean radius of precipitates at the onset of coarsening and time t, respectively, and k_r is a rate constant.

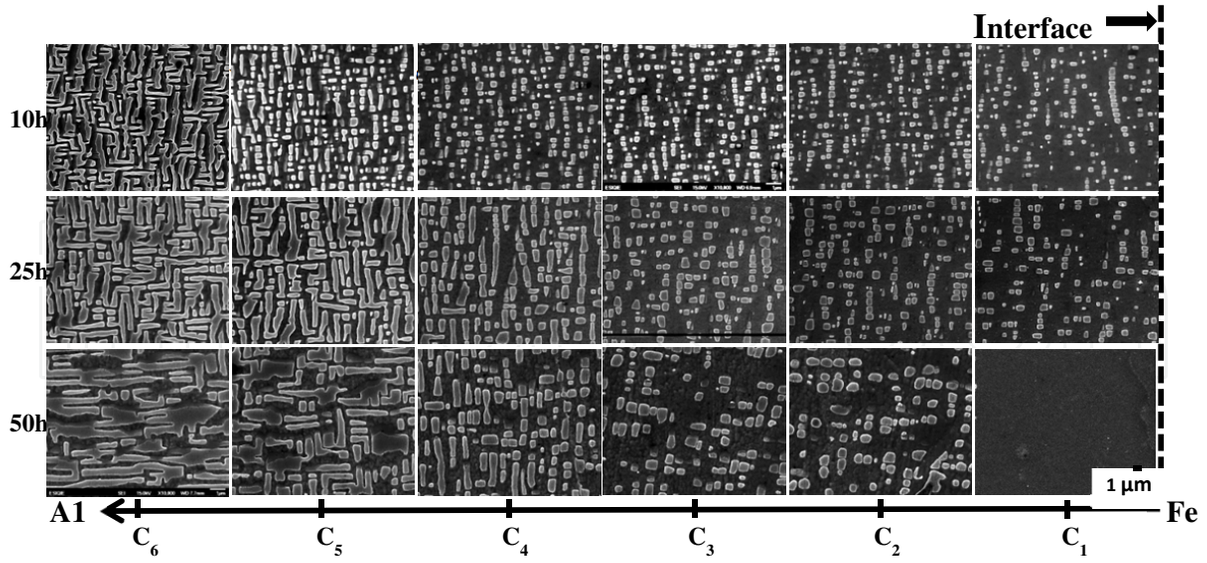

Figure 16. SEM micrographs of different positions in the diffusion couple.

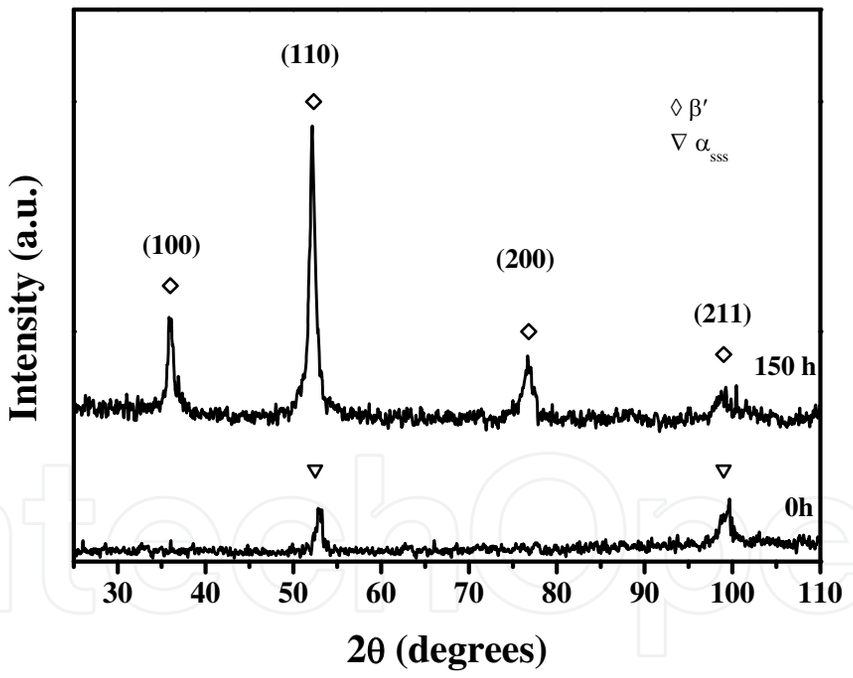

Figure 17. X-ray diffraction pattern of the diffusion couple.

Figure 19 shows the graph of r^3–r_o^3 against time t. The rate constant k_r for the coarsening process of β' phase in the ferritic matrix were determined from the slope of the straight lines and they are 2.4, 2.5, 3.0 and 3.90× 10^{-5} nm^3h^{-1} for the compositions C_1–C_4, respectively. These values are similar to those reported in the literature [14,15].

http://dx.doi.org/10.5772/61070

Position	Al (at.%)	Fe (at.%)	Ni (at.%)
C_1	11.16	76.87	11.98
C_2	13.91	72.71	13.39
C_3	15.09	70.12	14.88
C_4	20.0	61.67	18.33
C_5	23.24	54.26	22.5

Table 1. Chemical composition of selected positions

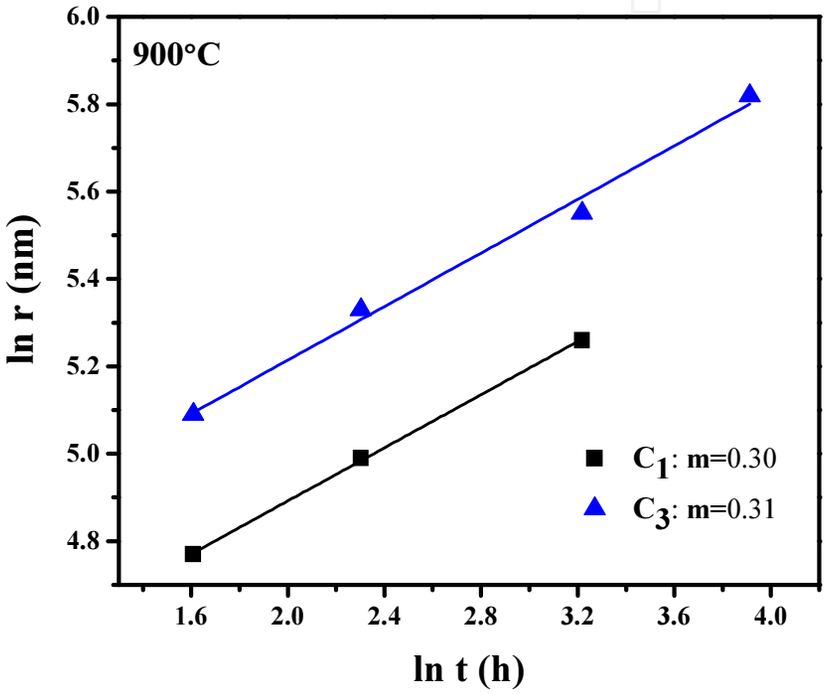

Figure 18. Plot of ln *r* versus ln *t*.

Figure 20 shows the precipitate size distributions for C_1 and C_4 compositions at different aging time along with the theoretical distribution functions predicted from the LSW theory. In these figures, the ordinates are $\varrho^2 f(\varrho)$ where ϱ represents the normalized particle size as defined by the LSW theory.

The particle size distributions are symmetric and sharp for short aging times, but they become broader and more asymmetric for prolonged aging times. This behavior has been described early [10,13] occurring in alloy systems with high volume fractions due to the presence of elastic interactions in alloy systems. Therefore, this fact is associated with the periodic formation of precipitate groups and the possible precipitate coalescence. Figure 21 shows the variation of the average radius *r* with the precipitate volume fraction for the diffusion couple after aging for 25 h. It is manifest the increase in the precipitate radius as the precipitate volume fraction increases because of the faster coarsening kinetics.

The plot of Vickers hardness versus Fe composition is shown in Figure 22 for the diffusion couple specimen aged at 900°C for different times. It can be noted that the hardness increases with the decrease in Fe content since the volume fraction of β' precipitates also shows an increase with the decrease in iron content or the increase in Ni and Al contents. The hardness of diffusion couple also increased with the aging time because of the coherent precipitates formed during the aging process.

In summary, the above results indicate that the hardness of the aged Fe-Ni-Al alloys show an increase with the increase in Al and Ni contents due to the increase in the volume fraction of β′ precipitates; nevertheless, the coarsening resistance decreases rapidly with the increase in Al and Ni contents due to the increase in the volume fraction of β′ precipitates. With the aim of having good coarsening resistance and the highest hardness in the Fe-rich aged Fe-Ni-Al alloys, the Ni and Al contents have to be lower than about 15 at.% Ni and 15 at.% Al, as stated by Figures 15 and 16. If higher contents of Al and Ni were necessary, the coarsening kinetics will be faster. In this case, it would be better to consider Ni-rich Fe-Ni-Al alloys with an austenite matrix and β′ precipitates which are expected to have higher coarsening resistances due to the lower atomic diffusion process in the fcc austenite phase than that in the bcc ferrite phase [2].

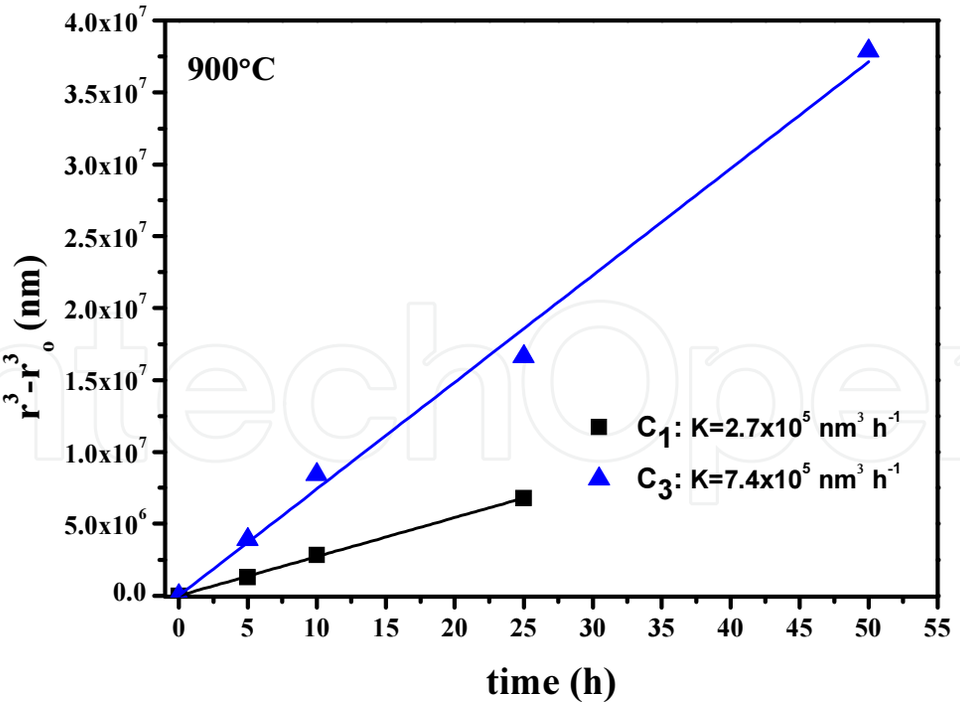

Figure 19. Plot of the cube equivalent radius as a function of aging time.

http://dx.doi.org/10.5772/61070

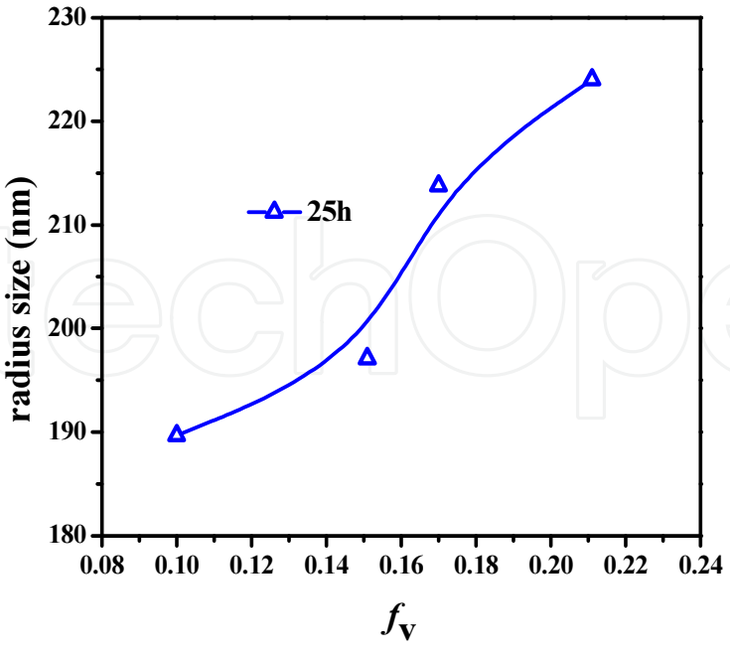

Figure 20. Radius as a function of volume fraction of precipitates.

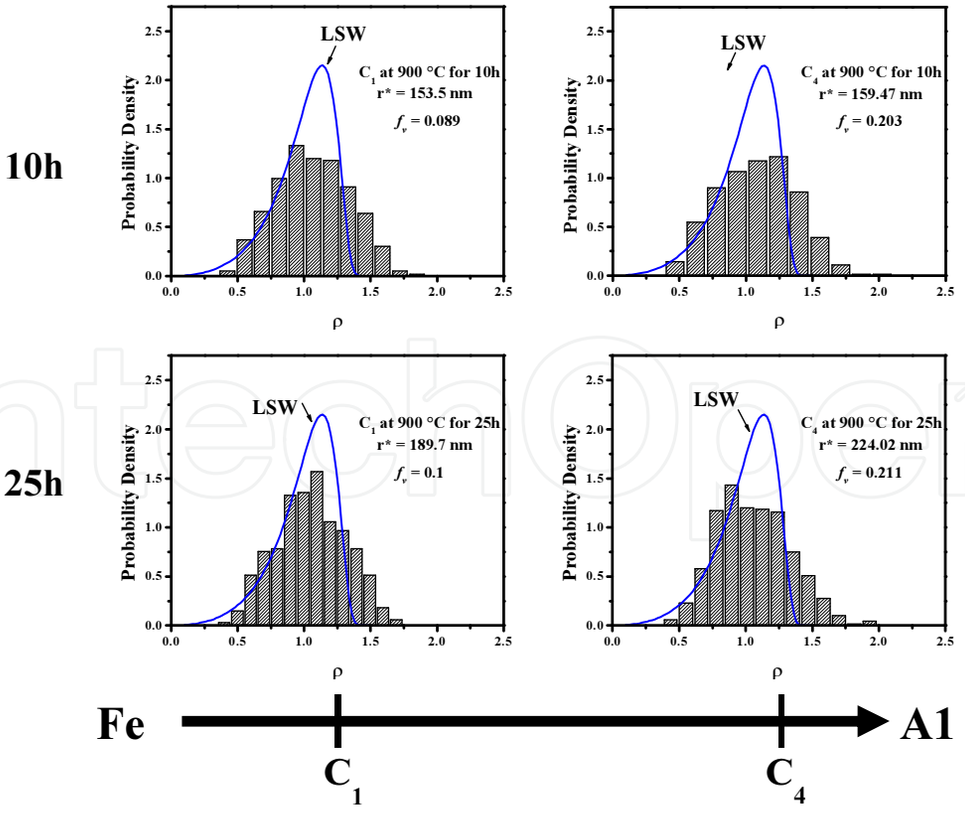

Figure 21. Precipitates size distribution for different compositions.

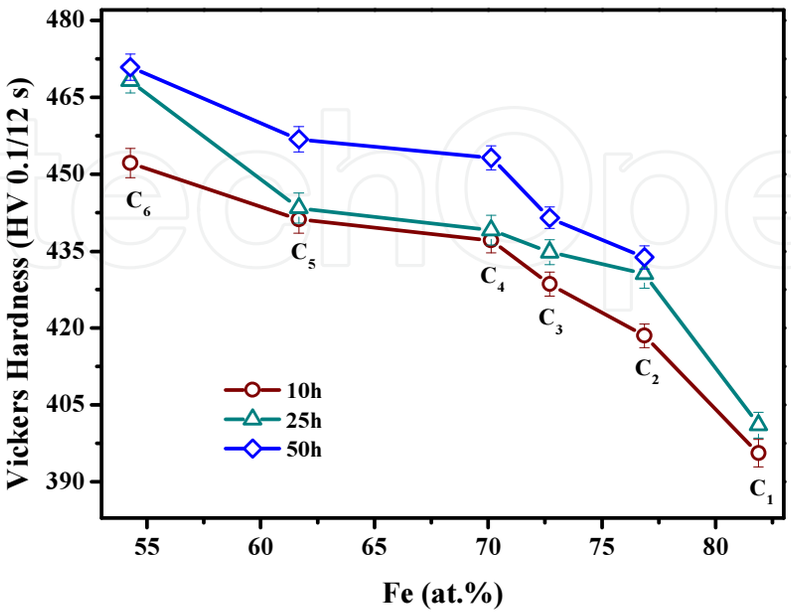

Figure 22. Plot of Vickers hardness versus at.% Fe.

8. Conclusions

An analysis of the precipitation evolution in the Fe-rich Fe-Ni-Al-based alloys was carried out using two different methods, the traditional way using one alloy composition and the diffusion couples which enables to analyze the precipitation in different alloy composition in the same specimen. This study indicates clearly the precipitation hardening of these alloys by the presence of the β′ phase precipitates in the ferrite phase matrix. The morphology of the β′ precipitates is rounded cuboids and it changes to elongated plates aligned in the <100> crystallographic direction. The coarsening growth kinetics of the β′ precipitates, in general, followed the modified LSW theories for diffusion-controlled coarsening. The addition of alloying elements such as copper or chromium promotes the increase in coarsening resistance and aging peak hardness by either its dissolution into the ferrite matrix or precipitates.

Acknowledgements

The authors wish to acknowledge financial support from, GAID, SIP-IPN and Conacyt.

Author details

Hector J. Dorantes-Rosales, Victor M. Lopez-Hirata*, Jorge L. Gonzalez-Velazquez, Nicolas Cayetano-Castro and Maribel L. Saucedo-Muñoz

*Address all correspondence to: vlopezhi@prodigy.net.mx

Instituto Politecnico Nacional (ESIQIE-CNMN), Department of Metallurgy and Materials, Mexico City, Mexico

References

[1] Guo Z, Sha W, Vaumosse D. Microstructural evolution in a PH13-8 stainless steel after ageing. Acta Mater 2003;51(1):101–16.

[2] Sauthoff G. Intermetallics. VCH 1995.

[3] Stalybrass C, Sauthof G. Ferritic Fe-Al-Ni-Cr alloys with coherent precipitates for high temperature applications. Mater Sci Eng 2004;A 387:985 –90.

[4] Stalybrass C, Schneider A, Sauthof G. The strengthening effect of (Ni,Fe)Al precipitates on the mechanical properties at high temperatures of ferritic FeNiAlCr alloys. Intermetallics 2005;13:1263 –8.

[5] Muñoz-Morris MA, Morris DG. Microstructure and mechanical behavior of a Fe-Ni-Al alloy. Mater Sci Eng 2007;444A:236 –41.

[6] Soriano-Vargas O, Saucedo-Muñoz ML, Lopez-Hirata VM, Paniagua-Mercado AM. Coarsening of β′ precipitates in an isothermally-aged Fe_{75}-Ni_{10}-Al_{15} alloy. Mater Trans JIM 2010;51:442 –6.

[7] Lifshitz IM, Slyozov VV. The kinetics of precipitation from supersaturated solid solution. J Phys Chem Solids 1961;19:35 –50.

[8] Wagner C. Theorie der alterung von niederssclagen durch umlosen. Z Electrochem 1961;65:581 –91.

[9] Baldan A. Progress in Ostwald ripening theories and their applications to nickel-base superalloys. J Mater Sci 2002;37:2171 –202.

[10] Kuehmann CJ, Voorhees PW. Ostwald ripening in ternary alloys. Met Mater Trans 1996;27A:937 –43.

[11] Thornton K, Akaiwa N, Voorhees PW. Large-scale simulations of Ostwald ripening in elastically stressed solids: I. Development of microstructure. Acta Mater 2004;52:1365 –78.

[12] Ardell AJ. The effect of volume fraction on particle coarsening: theoretical considerations. Acta Metall 1972;30:61 –71.

[13] Kostorz G. Phase transformations in materials. Wiley-VCH; 2001.

[14] Rosales-Dorantes HJ, Cayetano-Castro N, Lopez-Hirata VM, Saucedo-Muñoz ML, Villegas-Cardenas JD, Hernández-Santiago F. Coarsening process of coherent β′ precipitates in Fe-10wt.%Ni-15wt.%Al and Fe-10wt.%Ni-15wt.%Al-1wt.%Cu alloys. Mater Sci Technol.2013;29:1492 –8.

[15] Cayetano-Castro N, Saucedo-Muñoz ML, Dorantes-Rosales HJ, Gonzalez-Velazquez JL, Villegas-Cardenas JD, Lopez-Hirata VM. Ostwald ripening process of coherent β′ precipitates during aging in $Fe_{0.75}Ni_{0.10}Al_{0.15}$ and $Fe_{0.74}Ni_{0.10}Al_{0.15}Cr_{0.01}$ alloys. Adv Mater Sci Eng 5;1–7.

[16] Miyazaki T, Kobayashi S, Koyama T. Determination of the critical nucleus size of precipitates by utilizing the macroscopic composition gradient method. Met Trans 1999;30A:2783 –9.

[17] Miyazaki T, Koyama T, Kobayashi S. A new characterization method of the microstructure using the macroscopic composition gradient in alloys. Met Mater Trans 1996;26A:945 –9.

[18] Contreras-Piedras E, Dorantes-Rosales HJ, Lopez-Hirata VM, Hernandez-Santiago F, Gonzalez-Velazquez JL, Lopez –Monroy I. Analysis of precipitation in Fe-rich Fe-Ni-Al alloys by diffusion couples. Mater Sci Eng A 2012;558:366 –70.

[19] Thermo-Cal software 2008 v. 3.1/ Niv5.TDB.

[20] Hao S, Takayama T, Ishida K, Nishizawa T. Miscibility gap in Fe-Ni-Al and Fe-Ni-Al-Co systems. Met Trans 1984;15A:1819 –28.

[21] Mehrer H. Diffusion in Solid Metals and Alloys. Springer-Verlag, 1990.